



Synthesis of NiFe₂O₄ nanoparticles for removal of anionic dyes from aqueous solution

R. Zandipak^{a,*}, S. Sobhanardakani^b

^aYoung Researchers & Elite Club, Hamedan Branch, Islamic Azad University, Hamedan, Iran, Tel. +98 8134494143; email: raziye.zandi@yahoo.com

^bDepartment of the Environment, College of Basic Sciences, Hamedan Branch, Islamic Azad University, Hamedan, Iran, email: s_sobhan@iauh.ac.ir

Received 13 September 2014; Accepted 10 April 2015

ABSTRACT

NiFe₂O₄ nanoparticles (NiFe₂O₄ NPs) were synthesized and characterized using X-ray diffraction, transmission electronic microscopy (TEM), pH_{pzc} and Brunauer, Emmett, and Teller methods. Size of the nanostructures according to TEM was obtained around 12 nm. The prepared NiFe₂O₄ NPs was used as an adsorbent for the removal of anionic dyes of Sunset Yellow, Tartrazine, and Eriochrome Black T from aqueous solutions. It was found that removal percentage significantly depends on the level of initial solution pH. The adsorption of anionic dyes on to NiFe₂O₄ NPs was investigated from both equilibrium and kinetic point of view. Kinetic experiments were performed at three values of initial dyes concentration in the solution and the results of fitting to the experimental data by the non-linear methods represent that fractal-like pseudo-second-order model can describe the kinetics of adsorption. Among the various conventional isotherm models, Langmuir–Freundlich is more suitable for analyzing the explanation data. The adsorption capacities of Sunset Yellow, Tartrazine, and Eriochrome Black T on NiFe₂O₄ NPs were 107.1, 104.8, and 81.52 mg/g, respectively. Also, the method was applied to the removal of dyes in real samples (tap water, river water, and candy).

Keywords: NiFe₂O₄ nanoparticles; Anionic dyes; Adsorption; Kinetic; Isotherm

1. Introduction

The presence of dyes in wastewaters may cause serious problems to the environment because of their high toxicity to aquatic organisms and unfavorable aesthetical impact [1]. Organic dyes used in various industries, including the dyestuff, paper, leather, cosmetic, and textile [2,3]. Dyes can cause allergy, dermatitis, skin irritation, and also provoke cancer and mutation in humans [4]. Most of them are stable

to light and oxidizing agents because of their complex chemical structures. Dyes contaminate not only the environment but also traverse through the entire food chain, leading to biomagnifications. Thus, they should be carefully removed from the environment [5].

Various technologies, such as coagulation/flocculation, chemical oxidation, filtration, membrane separation, and microbial degradation, have shown limited success in the treatment of dye-containing wastewaters [6–8], and adsorption is considered to be the most effective technique for water and wastewater

*Corresponding author.

treatment, due to its simplicity, low cost, ease of operation, and high efficiency [9].

Most commercial systems currently use zeolite, activated carbon, industrial byproduct, agricultural waste, clay, biomass, and polymeric materials as adsorbent for this target. However, the application of these adsorbents is limited because of their low adsorption capacities and separation inconvenience. Thus, great efforts are needed to exploit new promising adsorbents [10–14].

Magnetic nanomaterials have attracted much interest because they not only have a large removal capacity, fast kinetics, and reactivity for contaminant removal, but also have high separation efficiency and reusability. In recent years, spinel ferrites with the general formula MFe_2O_4 ($M = Fe, Co, Cu, Mn, Ni, \text{etc.}$) have received much research attention, owing to both broad practical applications in several important technological fields such as ferrofluids, magnetic drug delivery, magnetic high-density information storage, and degradation of organic pollutants such as dye and halogenated derivatives in wastewater treatment [15,16].

$NiFe_2O_4$ nanoparticles ($NiFe_2O_4$ NPs) are known as an adsorbent because of their good biocompatibility, strong super paramagnetic property, low toxicity, easy preparation, and high adsorption ability [17]. $NiFe_2O_4$ NPs with an inverse spinel structure shows ferrimagnetism that originates from magnetic moment of anti-parallel spins between Fe^{3+} ions at tetrahedral sites and Ni^{2+} ions at octahedral sites. $NiFe_2O_4$ NPs exhibit high surface area and low mass transfer resistance. Moreover, the magnetic behavior of these nanoparticles depends mostly on their size [18]. Recently, some of the researchers have prepared $NiFe_2O_4$ NPs by different synthesis methods. Berthelin et al. have reported $NiFe_2O_4$ NPs with elementary particle size close to 4–5 nm by flash microwave synthesis [19]. Khosravi and Eftekhari [20] prepared $NiFe_2O_4$ NPs by sol-gel method. Wang et al. [21]

synthesized MFe_2O_4 ($M = Co, Ni$) ribbons with nanoporous structure which were prepared by electrospinning combined with sol-gel technology.

In the present study, the $NiFe_2O_4$ NPs was prepared as a magnetic adsorbent by the co-precipitation method and used for the removal of anionic dyes from water and food samples. Finally, the experimental data were modeled with non-linear isotherms and kinetics models. The effects of pH on the adsorption efficiency were studied too.

2. Experimental

2.1. Apparatus and reagents

The concentration of dye in the solutions was measured using a UV-vis spectrophotometer (Lambda 45, Perkin Elmer, Waltham, USA). All pH measurements were made with a 780 pH meter (Metrohm, Switzerland) combined with a glass-calomel electrode.

The crystal structure of synthesized materials was determined by an X-ray diffraction (XRD) (38066 Riva, d/G.via M. Misone, 11/D (TN) Italy) at ambient temperature. The structure of the $NiFe_2O_4$ NPs was characterized by a transmission electronic microscopy (TEM, Philips, CM10, 100 kV). Specific surface area and porosity were defined by N_2 adsorption-desorption porosimetry (77 K) using a porosimeter (Bel Japan, Inc.). The elemental analysis was measured by scanning electron microscope energy dispersive X-ray spectroscopy (SEM-EDX, XL 30 and Philips Netherland).

All chemicals and reagents used in this work were of analytical grade and purchased from Merck Company (Merck, Darmstadt, Germany). Stock solutions of dyes (10^{-3} M) were prepared by dissolving the appropriate amount of their powder in double-distilled water (DDW). DDW was used for preparation of all solutions. Fig. 1 shows the structure of the investigated dyes.

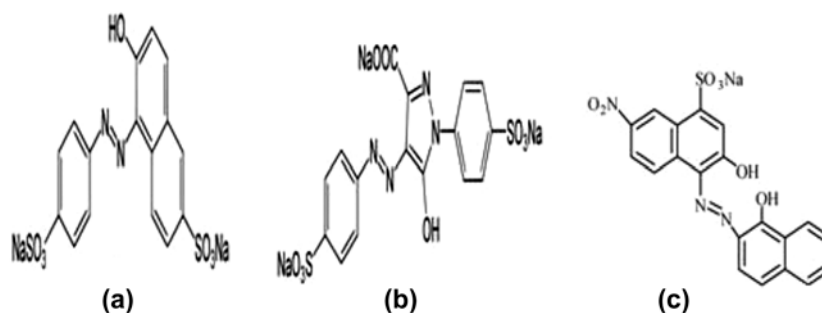


Fig. 1. Chemical structure of dye molecules (a) Sunset Yellow, (b) Tartrazine, and (c) Eriochrome Black T.

2.2. Synthesis of NiFe₂O₄ NPs

The NiFe₂O₄ samples were prepared by the co-precipitation method. In a typical synthesis, 0.2 M (20 mL) solution of iron nitrate [(Fe(NO₃)₃·9H₂O)] and 0.1 M (20 mL) solution of nickel nitrate [(Ni(NO₃)₂·6H₂O)] were prepared and vigorously mixed under stirring for 1 h at 80°C. 0.2 g of polyethylene oxide was added into the solution as a capping agent. Subsequently, 5 mL of hydrazine hydrate (NH₂·NH₂·H₂O) was added drop by drop into the solutions and brown color precipitates were formed. Finally, the precipitates were separated by centrifugation and dried in hot air oven for 4 h at 100°C. The acquired substance was annealed for 10 h at 300°C [22].

2.3. Point of zero charge pH

The point of zero charge pH (pH_{pzc}) for the adsorbents was determined by introducing 0.05 g of NiFe₂O₄ NPs into eight 100-mL Erlenmeyer flasks containing 0.1 M NaNO₃ solution. The pH values of the solutions were adjusted to 2, 3, 4, 5, 6, 7, 8, and 9 using solutions of 0.01 mol L⁻¹ HNO₃ and NaOH. The solution mixtures were allowed to equilibrate in an isothermal shaker (25°C) for 24 h. The final pH was measured after 24 h. The pH_{pzc} is the point where the pH_{initial} = pH_{final}.

2.4. Equilibrium and kinetic experiment

The equilibrium studies were carried out by adding 10 mL of different initial concentrations (10–220 mg/L) of Sunset Yellow, Tartrazine, and Eriochrome Black T solution to 0.05 g of adsorbent. The samples were shaken at 25°C and shaking speed of 160 rpm for 24 h to reach equilibrium condition. Then, the adsorbent was separated by an external magnet and the equilibrium concentration of Sunset Yellow, Tartrazine, and Eriochrome Black T in the bulk (C_e) was determined at 482, 430, and 530 nm, respectively, using a UV–vis spectrophotometer (Lambda 45, Perkin Elmer, USA) and the amount of adspecies at equilibrium, q_e (mg/g), was calculated by the following equation:

$$q_e = \frac{(C_0 - C_e)V}{W} \quad (1)$$

where C₀ and C_e (mg/L) are the initial and equilibrium concentrations, respectively, V (L) is the volume of solution, and W (g) is the mass of adsorbent.

The kinetic studies were performed at three different initial concentrations 15, 35, and 50 mg/L. For kinetic experiments, a series of 10 mL of dye solution was added to 0.05 g of adsorbent. The samples were placed in a shaker with 160 rpm and at 25°C. Then, samples were withdrawn at different time intervals and the concentrations of the dye that remained in the solution were determined by UV–vis spectrophotometer. The amount of dyes adsorbed per unit mass of adsorbent, at any time (q_t), was calculated by Eq. (2):

$$q_t = \frac{(C_0 - C_t)V}{W} \quad (2)$$

2.5. Effect of pH

To study the role of pH on the removal percentage of Sunset Yellow, Tartrazine, and Eriochrome Black T by NiFe₂O₄ NPs, 10 mL of dye solutions of concentration 15 mg/L in the pH range of 3–10 (using HCl and NaOH) were prepared. Then, 0.05 g of NiFe₂O₄ NPs was added and the solutions were shaken for 120 min. Then, the solutions were analyzed with UV–vis spectrophotometer. The removal percentage of dye was calculated by [23]:

$$R (\%) = \frac{C_0 - C_e}{C_0} \times 100 \quad (3)$$

2.6. Preparation of real samples

In order to demonstrate the applicability and reliability of the method for real samples, three samples, including tap water, river water, and candy sample were prepared and analyzed. Tap water samples were taken from our research laboratory (Islamic Azad University, Hamedan Branch, Iran), and river water were collected in a 2.0 L PTFE bottle. All water samples filtered through a filter paper (Whatman No. 40) to remove suspended particulate matter.

The candy sample (10 g) was ground with mortar in a pestle and subsequently dissolved in DDW. After mixing, the residue was filtered, diluted with DDW up to standard volume. The sample solution was then analyzed by the recommended procedure.

3. Results and discussion

3.1. Characterization of NiFe₂O₄

In order to better understand the adsorption behavior of NiFe₂O₄ NPs toward the dye molecule, a

fine characterization of their structural properties was performed. The XRD pattern of NiFe₂O₄ NPs is shown in Fig. 2. Furthermore, it can be seen that all the diffraction peaks of NiFe₂O₄ may be assigned to spinel-type NiFe₂O₄ (JCPDS 54-0964). The peaks at the 2θ values of 30.1°, 35.3°, 43.0°, 53.7°, 56.5°, and 62.4° can be indexed to (1 1 1), (2 2 0), (3 1 1), (4 0 0), (4 2 2), (5 1 1), and (4 4 0) crystal planes of spinel NiFe₂O₄, respectively. The average crystallite size (D in nm) of NiFe₂O₄ NPs was determined from XRD pattern according to the Scherrer equation.

$$D = \frac{K\lambda}{\beta \cos \theta} \quad (4)$$

where λ is the wavelength of the X-ray radiation (1.5406 Å), K is a constant taken as 0.89, θ is the

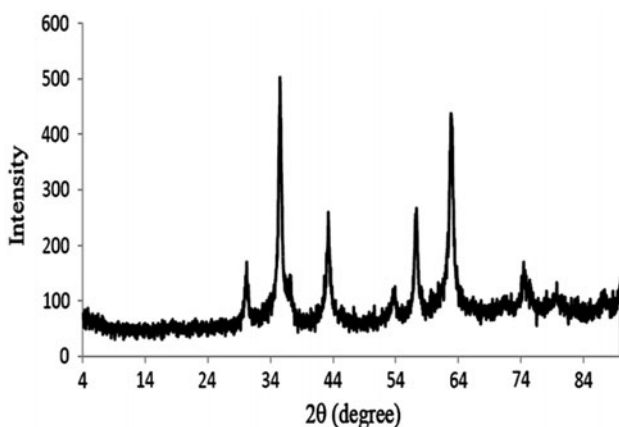


Fig. 2. The X-ray diffraction pattern of NiFe₂O₄ NPs.

diffraction angle, and β is the full width at half maximum. The average size of the NiFe₂O₄ NPs was calculated as around 15 nm. The TEM micrograph and calculated histogram of the NiFe₂O₄, as shown in Fig. 3, revealed that the diameter of the synthesized NiFe₂O₄ NPs was around 12 nm. The particle size measured directly from the TEM micrograph agrees with that determined by the XRD results. Fig. 4 shows a typical SEM-EDX elemental analysis of NiFe₂O₄ NPs. The results demonstrate that only Ni, Fe, and O appear in NiFe₂O₄ NPs samples. Also, the results have a good agreement with other reported.

Specific surface areas are commonly reported as BET surface areas obtained by applying the theory of Brunauer, Emmett, and Teller (BET) to nitrogen adsorption/desorption isotherms measured at 77 K. This is a standard procedure for the determination of the specific surface area of sample. The specific surface area of the sample is determined by physical adsorption of a gas on the surface of the solid and by measuring the amount of adsorbed gas corresponding to a monomolecular layer on the surface. The data are treated according to the BET theory [24]. The results of the BET method showed that the average specific surface area of NiFe₂O₄ NPs was 63.7 m² g⁻¹. It can be concluded from these values that the synthesized nanoparticles have relatively large specific surface areas and may be better for adsorption.

3.2. Adsorption isotherms modeling

The adsorption isotherm indicates how the adsorption molecules distribute between the liquid phase and the solid phase when the adsorption process reaches an equilibrium state. The equilibrium

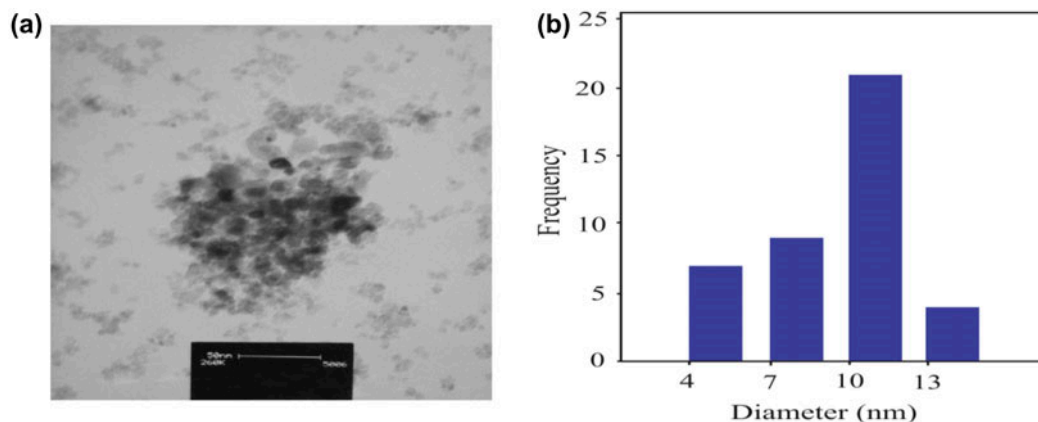


Fig. 3. (a) TEM micrograph and (b) calculated histogram of NiFe₂O₄ NPs.

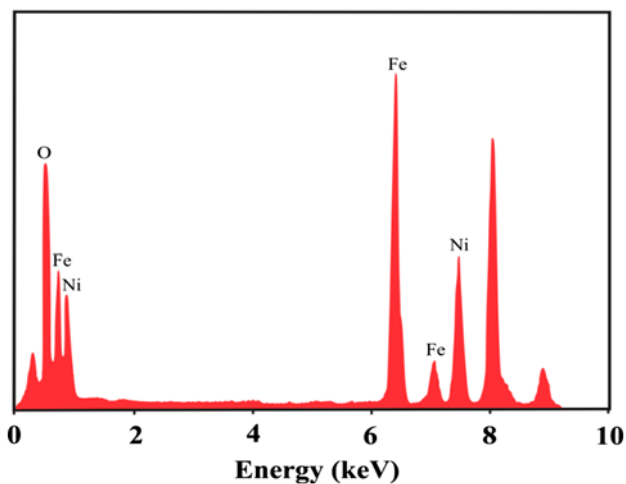


Fig. 4. SEM-EDX spectrum of NiFe_2O_4 NPs.

experimental data were analyzed with different models, including Langmuir (L), Freundlich (F), Temkin (T), Redlich–Peterson (R–P), and Langmuir–Freundlich (L–F) isotherms.

The Langmuir isotherm includes several assumptions which are surface homogeneity and absence of interactions between adsorbed molecules on the surface [25]. The non-linear form of Langmuir isotherm is given as follows:

$$q_e = \frac{q_m k_L C_e}{1 + k_L C_e} \quad (5)$$

where q_{\max} (mg/g) and K_L (L/mg) are known as Langmuir constants and referred to maximum adsorption capacity and affinity of adsorption, respectively.

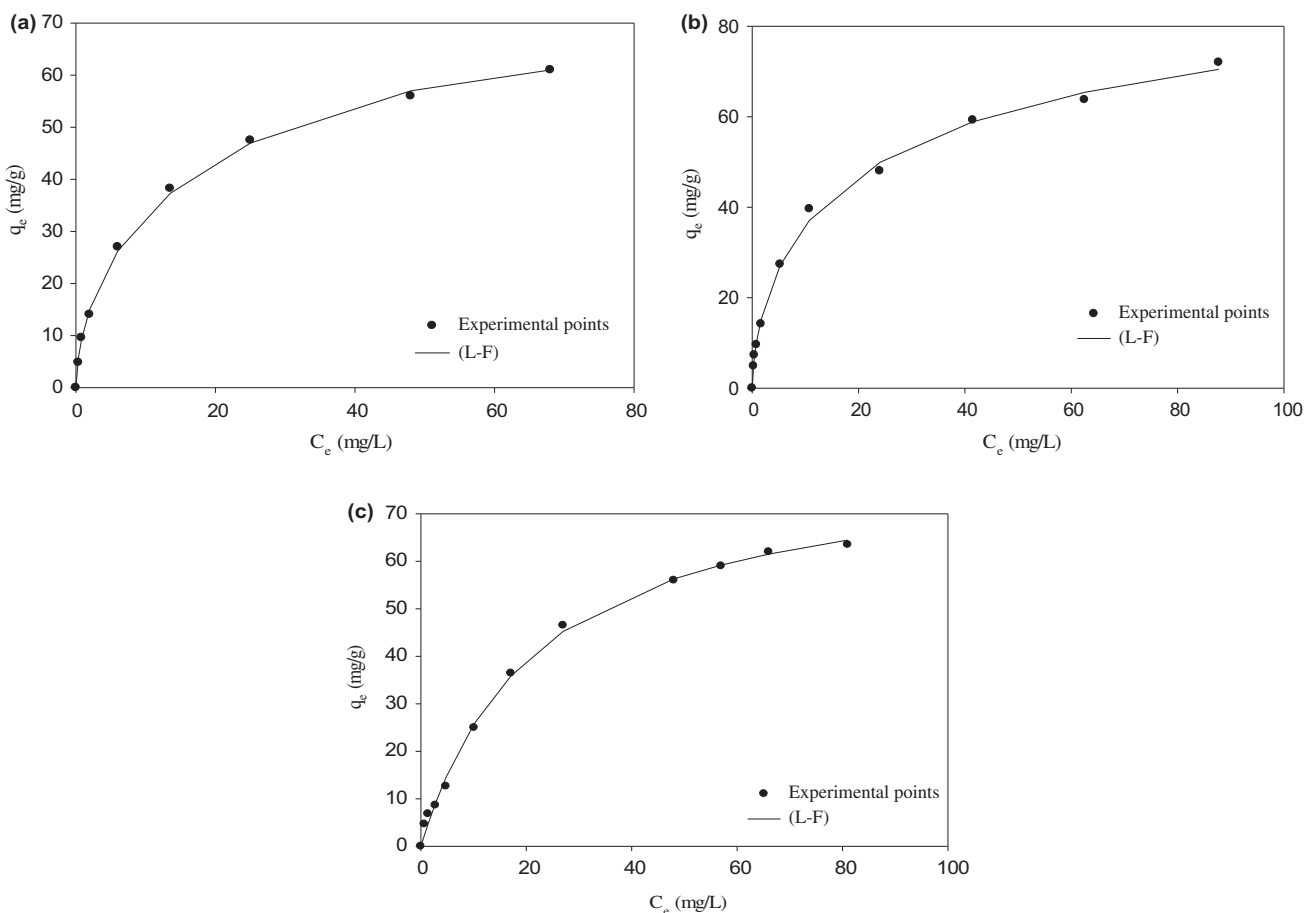


Fig. 5. Adsorption isotherm of (a) Sunset Yellow, (b) Tartrazine, and (c) Eriochrome Black T on to NiFe_2O_4 NPs.

The Freundlich isotherm is an empirical equation, utilizing for heterogeneous surfaces [26]. The non-linear form of Freundlich isotherm presented as follows:

$$q_e = k_f(C_e)^{1/n} \quad (6)$$

where K_F ($\text{mg}^{1-(1/n)} \text{L}^{1/n}/\text{g}$) is the Freundlich constant and n indicating the adsorption heterogeneity.

The Temkin isotherm model is [27]:

$$q_e = B \ln(AC_e) \quad (7)$$

where $B = RT/b$ and b (J mol^{-1}) is the Temkin constant related to the heat of adsorption; A (L/mg) is the Temkin isotherm constant.

Redlich–Peterson (R–P) is one of the three parameter equations [28]:

$$q_e = \frac{k_{R-P}C_e}{1 + \alpha C_e^\beta} \quad (8)$$

where k_{R-P} (L/g), α , and β are the Redlich–Peterson constants. β is the parameter which is between 0 and 1.

The other isotherm model used for modeling of equilibrium adsorption data is Langmuir–Freundlich isotherm [29]:

$$q_e = \frac{q_m(k_{L-F}C_e)^{1/n}}{1 + (k_{L-F}C_e)^{1/n}} \quad (9)$$

where K_{L-F} (L/mg) and n are the constants.

Fig. 5 displays the adsorption isotherms of three anionic dyes on the adsorbent at 25°C. The experimental data reveal that the equilibrium adsorption capacity of the dyes increases by increasing the initial dye concentration and finally reaches to the saturation value (q_m). The constant parameters of the isotherm equations which were obtained by non-linear method for this adsorption process and the correlation coefficients (r^2) for all applied isotherms are summarized in Table 1. It was found that Langmuir–Freundlich isotherm model shows high correlation coefficients ($r^2 > 0.99$) and lower RMS error than other models. Following of adsorption equilibrium data with Langmuir–Freundlich isotherm indicates a heterogeneous surface. Maximum adsorption capacity of 107.1, 104.8, and 81.52 mg/g

Table 1
Obtained parameters for adsorption of dyes on to NiFe_2O_4 NPs

Isotherm	Parameters	Anionic dyes		
		Sunset Yellow	Tartrazine	Eriochrome Black T
L	q_m (mg/g)	72.21	75.88	82.04
	K_L (L/mg)	0.092	0.109	0.045
	r^2	0.9796	0.9816	0.9972
	RMS error	3.644	3.546	1.340
	K_F ($\text{L mg}^{(1-(1/n))}/\text{g}$)	12.97	14.00	8.395
F	n	0.377	0.374	0.473
	r^2	0.9857	0.9838	0.9743
	RMS error	3.047	3.414	4.113
	B	11.69	11.56	14.07
T	A	2.565	3.455	0.992
	r^2	0.9687	0.9673	0.9488
	RMS error	4.506	4.857	5.810
	q_m (mg/g)	107.1	104.8	81.52
L–F	K_{L-F} (L/mg)	0.026	0.035	0.046
	n	1.626	1.59	0.990
	r^2	0.9958	0.9973	0.9979
	RMS error	1.568	1.273	1.331
	K_{R-P} (L/g)	18.02	20.40	3.514
R–P	α' ($\text{L}/\text{mg})^{1/\beta}$	0.782	0.788	0.034
	β	0.748	0.663	1.049
	r^2	0.9942	0.9971	0.9972
	RMS error	1.824	1.539	1.412

Table 2

Comparison of maximum adsorption capacity (q_m) of different adsorbents for dyes

Adsorbent	Maximum adsorption capacity (mg g^{-1})			Ref.
	Sunset Yellow	Tartrazine	Eriochrome Black T	
Chitin	–	30	–	[30]
Copper sulfide nanoparticles loaded on activated carbon	122	–	–	[31]
<i>Scolymus hispanicus</i> L	–	–	120.4	[32]
Rice hull-based activated carbon	–	–	160.3	[33]
ZnO nanoparticle loaded on activated carbon	142.8	–	–	[34]
Magnetic polymer multi-wall carbon nanotube	85.4	–	–	[35]
Nickel-doped zinc oxide	–	35.9	–	[36]
β -cyclodextrin/polyurethane	–	–	20.1	[37]
Hen feather	–	6.4×10^{-5}	–	[38]
NiFe ₂ O ₄ NPs	107.1	–	–	This work
NiFe ₂ O ₄ NPs	–	104.8	–	This work
NiFe ₂ O ₄ NPs	–	–	81.52	This work

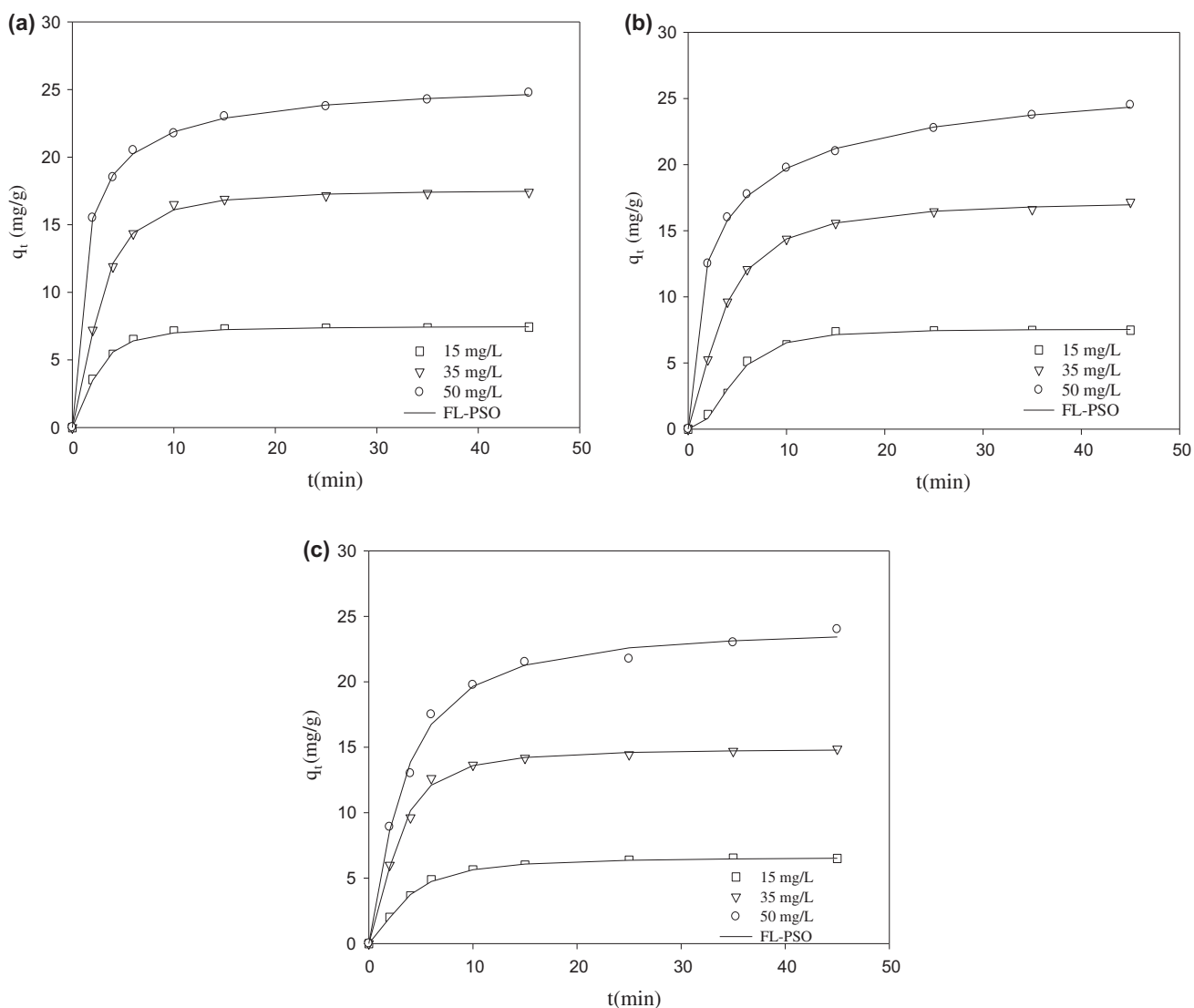


Fig. 6. Experimental kinetic data for the adsorption of (a) Sunset Yellow, (b) Tartrazine, and (c) Eriochrome Black T by NiFe₂O₄ NPs at different initial concentrations. Lines represent the FL-PSO model fitted with the data.

was obtained for Sunset Yellow, Tartrazine, and Eriochrome Black T dyes, respectively. In Table 2, we compared the ability of the proposed adsorbent in removal of anionic dyes from water with some other works.

3.3. Adsorption kinetics modeling

Adsorption kinetics provides information about the mechanism of adsorption and potential controlling

steps, which are essential for the practical design of adsorption systems.

Fig. 6 presents the variation in the adsorption of dyes as a function of contact time. From these figures, it is clearly seen that the dyes removal has been performed within the first 10 min which indicates that the rate of dyes adsorption by NiFe₂O₄ NPs is high. It is clear that the adsorption rate and the amount of adsorbed increase by increasing the initial concentration.

In order to predict the adsorption behavior of Sunset Yellow, Tartrazine, and Eriochrome Black T on

Table 3
Constant of kinetic models for adsorption of Sunset Yellow on to NiFe₂O₄ NPs

Kinetic model	C ₀ (mg/L)	a	α	k'	b	k ₁ (1/min)	k ₂ (g/mg min)	q _e (mg/g)	q _e (exp)	r ²	RMS error
PFO	15	–	–	–	–	0.334	–	7.37	–	0.9841	0.338
	35	–	–	–	–	0.285	–	17.31	–	0.9829	0.838
	50	–	–	–	–	0.450	–	23.34	–	0.9789	1.204
PSO	15	–	–	–	–	–	0.063	8.02	–	0.9995	0.058
	35	–	–	–	–	–	0.021	19.09	–	0.9991	0.187
	50	–	–	–	–	–	0.030	25.07	–	0.9987	0.294
E	15	0.904	–	–	34.38	–	–	–	–	0.9427	0.643
	35	0.334	–	–	37.15	–	–	–	–	0.9404	1.566
	50	0.350	–	–	47.00	–	–	–	–	0.9931	0.688
FL-PSO	15	–	1.750	0.034	–	–	–	7.48	–	0.9986	0.107
	35	–	1.730	0.011	–	–	–	17.59	–	0.9991	0.206
	50	–	0.792	0.032	–	–	–	26.06	–	0.9996	0.160
Experimental data	15	–	–	–	–	–	–	–	7.12	–	–
	35	–	–	–	–	–	–	–	17.15	–	–
	50	–	–	–	–	–	–	–	24.33	–	–

Table 4
Constant of kinetic models for adsorption of Tartrazine on to NiFe₂O₄ NPs

Kinetic model	C ₀ (mg/L)	a	α	k'	b	k ₁ (1/min)	k ₂ (g/mg min)	q _e (mg/g)	q _e (exp)	r ²	RMS error
PFO	15	–	–	–	–	0.148	–	7.70	–	0.9410	0.773
	35	–	–	–	–	0.204	–	16.70	–	0.9900	0.631
	50	–	–	–	–	0.308	–	22.59	–	0.9652	1.522
PSO	15	–	–	–	–	–	0.017	9.20	–	0.9693	0.557
	35	–	–	–	–	–	0.013	19.03	–	0.9975	0.313
	50	–	–	–	–	–	0.017	24.89	–	0.9951	0.567
E	15	0.459	–	–	2.288	–	–	–	–	0.9005	1.004
	35	0.270	–	–	11.66	–	–	–	–	0.9598	1.271
	50	0.264	–	–	61.09	–	–	–	–	0.9972	0.431
FL-PSO	15	–	2.460	0.002	–	–	–	7.56	–	0.9954	0.232
	35	–	1.499	0.008	–	–	–	17.32	–	0.9997	0.115
	50	–	0.647	0.018	–	–	–	28.38	–	0.9996	0.159
Experimental data	15	–	–	–	–	–	–	–	6.37	–	–
	35	–	–	–	–	–	–	–	16.45	–	–
	50	–	–	–	–	–	–	–	23.75	–	–

NiFe₂O₄ NPs surface, different adsorption kinetic models were applied for modeling experimental data at different initial concentrations.

Pseudo-first-order equation (PFO) is one of the most popular and empirical models for adsorption kinetics which presented by Lagergren [39]. The integrated form of this model can be given as follows:

$$q_t = q_e(1 - \exp(-k_1 t)) \quad (10)$$

where q_t and q_e (mg/g) are the amount of adsorbed species per unit mass of adsorbent at any time (t) and at equilibrium, respectively. k_1 (min⁻¹) is the pseudo-first-order rate constant.

Another simple and well-known kinetic model which is used extensively in recent years is pseudo-second-order equation (PSO) [39]. The integrated form of this equation is:

$$q_t = \frac{k_2 q_e^2 t}{1 + k_2 q_e t} \quad (11)$$

where k_2 (g/mg min) is the rate coefficient.

In order to investigate the adsorption of pollutants from aqueous solution, Elovich rate equation (E) has been widely used [40]. The integrated form of Elovich equation is expressed as follows:

$$q_t = \frac{1}{a} \ln(1 + abt) \quad (12)$$

where a and b are the equation constants. Mainly, Elovich equation is applied to describe chemical adsorption onto heterogeneous adsorbent surfaces.

One of the recently developed kinetic models for adsorption is the fractal-like pseudo-second-order model (FL-PSO), which was presented for the systems with different paths of adsorption [41]. The integrated form of this equation is:

$$q_t = \frac{k' q_e^2 t^\alpha}{1 + k' q_e t^\alpha} \quad (13)$$

where k' is the constant.

The experimental adsorption kinetic data were modeled with the mentioned models using non-linear fitting method. The results of fitting and also correlation coefficients (r^2) and RMS errors are presented in Tables 3–5.

The obtained correlation coefficients indicate that the adsorption kinetic data on NiFe₂O₄ NPs follow the FL-PSO model. Following of adsorption kinetic data with the FL-PSO model indicates that the rate coefficient of adsorption is a function of time. Time dependency of rate coefficient in fractal-like approach means that there are different paths for adsorption. The FL-PSO kinetic model presumes that surface is heterogeneous too.

3.4. Effect of solution pH

The pH of the dye solution affects the surface charge of the adsorbent, the degree of ionization of

Table 5
Constant of kinetic models for adsorption of Eriochrome Black T on to NiFe₂O₄ NPs

Kinetic model	C ₀ (mg/L)	a	α	k'	b	k_1 (1/min)	k_2 (g/mg min)	q_e (mg/g)	q_e (exp)	r^2	RMS error
PFO	15	–	–	–	–	0.209	–	6.45	–	0.9849	0.301
	35	–	–	–	–	0.280	–	14.65	–	0.9808	0.755
	50	–	–	–	–	0.225	–	22.74	–	0.9817	0.730
PSO	15	–	–	–	–	–	0.035	7.34	–	0.9964	0.147
	35	–	–	–	–	–	0.024	16.20	–	0.9961	0.338
	50	–	–	–	–	–	0.011	25.66	–	0.9921	0.711
E	15	0.707	–	–	4.718	–	–	–	–	0.9502	0.548
	35	0.385	–	–	28.07	–	–	–	–	0.9398	1.337
	50	0.213	–	–	21.43	–	–	–	–	0.9695	1.482
FL-PSO	15	–	1.622	0.020	–	–	–	6.61	–	0.9991	0.079
	35	–	1.737	0.012	–	–	–	14.89	–	0.9970	0.322
	50	–	1.272	0.009	–	–	–	24.23	–	0.9950	0.644
Experimental data	15	–	–	–	–	–	–	–	5.62	–	–
	35	–	–	–	–	–	–	–	14.17	–	–
	50	–	–	–	–	–	–	–	23.00	–	–

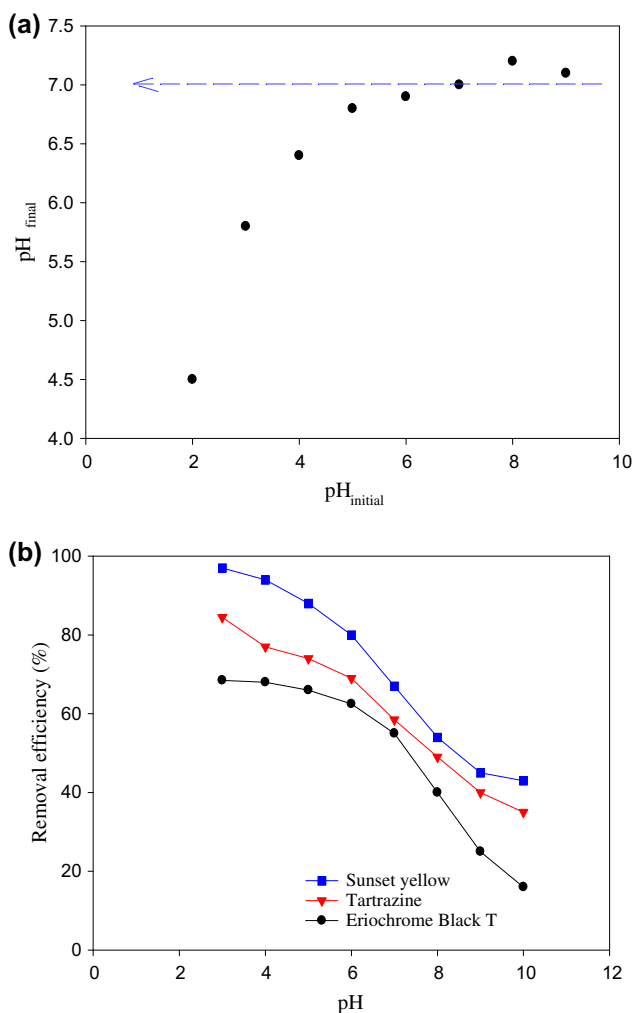


Fig. 7. (a) The determination of the point of zero charge of the $NiFe_2O_4$ NPs, and (b) effect of solution pH on the removal percentage of dyes by $NiFe_2O_4$ NPs.

the adsorbate molecules, and the extent of dissociation of the functional groups on the active sites of the adsorbent. The effects of initial pH on the percentage of removal of anionic dyes using $NiFe_2O_4$ NPs adsorbent were evaluated within the pH range between 3 and 10 (Fig. 7(b)). Fig. 7(b) demonstrates that the removal efficiency for anionic dyes (Sunset Yellow, Tartrazine, and Eriochrome Black T) gradually decreased with increase in pH.

The point of zero charge (pH_{pzc}) is an important property that indicates the electrical neutrality of the surface of the adsorbent at a particular value of pH.

As observed in Fig. 7(a), the pH_{pzc} for $NiFe_2O_4$ NPs is 7.0. At pH values below the pH_{pzc} , the surface of $NiFe_2O_4$ NPs is positively charged and the electrostatic interaction between the cationic charged $NiFe_2O_4$ NPs surface and the sulfonate anions of negatively dye molecules was increased, which led to the increase in adsorption capacity. This interaction enhanced by van der Waals force as extra interaction bond. At pH values higher than the pH_{pzc} , the surface charge is negative and by increasing of pH, the negative charge on the surface increases. Therefore, by increasing of pH from 3 to 10, the removal efficiency decreases because of repulsion forces between anionic dyes.

3.5. Adsorption of anionic dyes in real samples

A standard addition method was applied to the adsorption of anionic dyes of Sunset Yellow, Tartrazine, and Eriochrome Black T in real samples using $NiFe_2O_4$ NPs. The samples were also analyzed after spiking with different concentrations of dyes. Tap water, river water, and candy samples were analyzed. The results are given in Table 6. The recovery studies of the spiked dyes in different samples showed average values in the range from 92.6 to 101%. The results indicate the applicability of the $NiFe_2O_4$ NPs for dyes adsorption in samples and also the method is suitable for the analysis of real samples.

3.6. Desorption studies

Desorption studies is very important in developing a novel adsorbent for use in practical applications. In the present study, desorption experiment was carried out with different eluents such as methanol, ethanol, acetic acid, NaOH, and mixture of methanol and sodium hydroxide. For this purpose, 10 mL of desorbent solution was added to the 0.05 g dye-loaded $NiFe_2O_4$ NPs in a beaker. The nanoparticles were collected magnetically from the solution. The concentration of dyes in the desorbed solution was measured by UV-vis spectrophotometry. The results are given in Fig. 8. As the results show, the desorption efficiencies for mixture of methanol and sodium hydroxide were higher than other solutions. Also, the reusability of the adsorbent was greater than four cycles without any loss in its adsorption behavior.

Table 6

Results of adsorption of anionic dyes in various real samples using NiFe₂O₄ NPs adsorbent under the optimum conditions ($n = 5$)

Sample	Dyes	Added ($\mu\text{g L}^{-1}$)	Found ($\mu\text{g L}^{-1}$)	Recovery (%)
Tap water	Sunset Yellow	20	19.7	98.5
		30	28.8	96
	Tartrazine	20	19.5	97.5
		30	30.3	101
	Eriochrome Black T	20	19.9	99.5
		30	30.1	100.3
River water	Sunset Yellow	20	18.8	94
		30	29.9	99.6
	Tartrazine	20	19.6	98
		30	29.4	98
	Eriochrome Black T	20	19.1	95.5
		30	29.7	99
Candy	Sunset Yellow	15	14.1	94
		40	39.5	98.7
	Tartrazine	15	14.7	98
		40	39.9	99.7
	Eriochrome Black T	15	13.9	92.6
		40	39.7	99.2

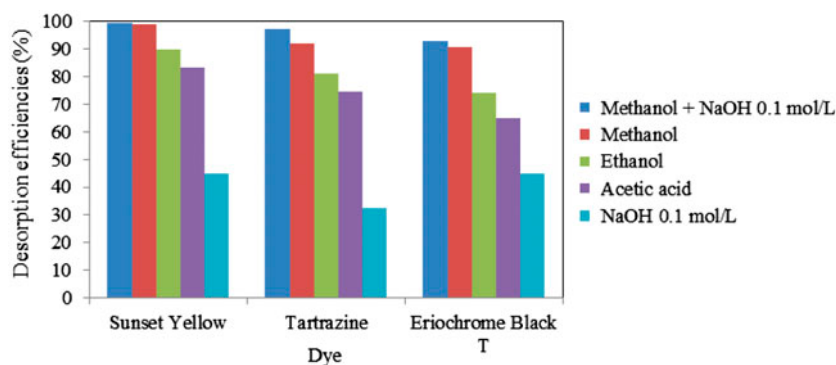


Fig. 8. Effect of type of eluting agent on recovery (%) for anionic dyes adsorbed on NiFe₂O₄ NPs.

4. Conclusion

In summary, NiFe₂O₄ nanoparticles are synthesized by co-precipitation method. The size of the product was determined by XRD analysis and TEM. The NiFe₂O₄ NPs showed an excellent ability to remove different dyes (Sunset Yellow, Tartrazine, and Eriochrome Black T) within 10 min from water samples. The highest removal percentage for dyes was observed at acidic pH. The equilibrium data are analyzed using Langmuir, Freundlich, Temkin, Redlich–Peterson, and Langmuir–Freundlich isotherm equations. The result shows that the experimental data are best correlated by Langmuir–Freundlich isotherm. The kinetic studies reveal that the rate of adsorption onto NiFe₂O₄ NPs is rapid. Also, following of adsorption kinetic data by FL-PSO model indicates that the

rate coefficient changes with time. Also, removal efficiency was found to be 97.9, 96.5, and 93.5% for Sunset Yellow, Tartrazine, and Eriochrome Black T, respectively, demonstrating the high efficiency of the NiFe₂O₄ NPs for the anionic dyes adsorption in aqueous solutions.

References

- [1] W.J. Tseng, R.D. Lin, BiFeO₃/α-Fe₂O₃ core/shell composite particles for fast and selective removal of methyl orange dye in water, *J. Colloid. Interface Sci.* 428 (2014) 95–100.
- [2] Y.R. Zhang, S.L. Shen, S.Q. Wang, J. Huang, P. Su, Q.R. Wang, B.X. Zhao, A dual function magnetic nanomaterial modified with lysine for removal of organic dyes from water solution, *Chem. Eng. J.* 239 (2014) 250–256.

- [3] H. Gao, S. Zhao, X. Cheng, X. Wang, L. Zheng, Removal of anionic azo dyes from aqueous solution using magnetic polymer multi-wall carbon nanotube nanocomposite as adsorbent, *Chem. Eng. J.* 223 (2013) 84–90.
- [4] L.G. da Silva, R. Ruggiero, P.M. Gontijo, R.B. Pinto, B. Royer, E.C. Lima, T.H.M. Fernandes, T. Calvete, Adsorption of Brilliant Red 2BE dye from water solutions by a chemically modified sugarcane bagasse lignin, *Chem. Eng. J.* 168 (2011) 620–628.
- [5] J. Goscianska, M. Marciniak, R. Pietrzak, Mesoporous carbons modified with lanthanum(III) chloride for methyl orange adsorption, *Chem. Eng. J.* 247 (2014) 258–264.
- [6] T. Soltani, M.H. Entezari, Sono-synthesis of bismuth ferrite nanoparticles with high photocatalytic activity in degradation of Rhodamine B under solar light irradiation, *Chem. Eng. J.* 223 (2013) 145–154.
- [7] M. Khayet, A.Y. Zahrim, N. Hilal, Modelling and optimization of coagulation of highly concentrated industrial grade leather dye by response surface methodology, *Chem. Eng. J.* 167 (2011) 77–83.
- [8] T.H. Kim, C. Park, J. Yang, S. Kim, Comparison of disperse and reactive dye removals by chemical coagulation and Fenton oxidation, *J. Hazard. Mater.* 112 (2004) 95–103.
- [9] J. Galán, A. Rodríguez, J.M. Gómez, S.J. Allen, G.M. Walker, Reactive dye adsorption onto a novel mesoporous carbon, *Chem. Eng. J.* 219 (2013) 62–68.
- [10] S. Sobhanardakani, H. Parvizimosaed, E. Olyaie, Heavy metals removal from wastewaters using organic solid waste—Rice husk, *Environ. Sci. Pollut. Res.* 20 (2013a) 5265–5271.
- [11] X. Li, Y. Li, S. Zhang, Z. Ye, Preparation and characterization of new foam adsorbents of poly(vinylalcohol)/chitosan composites and their removal for dye and heavy metal from aqueous solution, *Chem. Eng. J.* 183 (2012) 88–97.
- [12] E. Errais, J. Duplay, F. Darragi, I. M'Rabet, A. Aubert, F. Huber, G. Morvan, Efficient anionic dye adsorption on natural untreated clay: Kinetic study and thermodynamic parameters, *Desalination* 275 (2011) 74–81.
- [13] S. Azizian, M. Haerifar, H. Bashiri, Adsorption of methyl violet onto granular activated carbon: Equilibrium, kinetics and modeling, *Chem. Eng. J.* 146 (2009) 36–41.
- [14] S.K. Alpat, Özge Özbayrak, Şenol Alpat, H. Akçay, The adsorption kinetics and removal of cationic dye, Toluidine Blue O, from aqueous solution with Turkish zeolite, *J. Hazard. Mater.* 151 (2008) 213–220.
- [15] H. Teymourian, A. Salimi, S. Khezrian, Fe₃O₄ magnetic nanoparticles/reduced graphene oxide nanosheets as a novel electrochemical and bioelectrochemical sensing platform, *Biosens. Bioelectron.* 49 (2013) 1–8.
- [16] I. Khosravi, M. Yazdanbakhsh, E.K. Goharshadi, A. Youssefi, Preparation of nanospinels NiMn_xFe_{2-x}O₄ using sol-gel method and their applications on removal of azo dye from aqueous solutions, *Mater. Chem. Phys.* 130 (2011) 1156–1161.
- [17] M. Yazdanbakhsh, I. Khosravi, E.K. Goharshadi, A. Youssefi, Fabrication of nanospinel ZnCr₂O₄ using sol-gel method and its application on removal of azo dye from aqueous solution, *J. Hazard. Mater.* 184 (2010) 684–689.
- [18] J.Y. Patil, D.Y. Nadargi, J.L. Gurav, I.S. Mulla, S.S. Suryavanshi, Synthesis of glycine combusted NiFe₂O₄ spinel ferrite: A highly versatile gas sensor, *Mater. Lett.* 124 (2014) 144–147.
- [19] C.B. Bousquet-Berthelin, D. Chaumont, D. Stuerger, Flash microwave synthesis of trevorite nanoparticles, *J. Solid State Chem.* 181 (2008) 616–622.
- [20] I. Khosravi, M. Eftekhari, Characterization and evaluation catalytic efficiency of NiFe₂O₄ nano spinel in removal of reactive dye from aqueous solution, *Powder Technol.* 250 (2013) 147–153.
- [21] Z. Wang, X. Liu, M. Lv, P. Chai, Y. Liu, J. Meng, Preparation of ferrite MFe₂O₄ (M = Co, Ni) ribbons with nanoporous structure and their magnetic properties, *J. Phys. Chem. B* 112 (2008) 11292–11297.
- [22] P. Sivakumar, R. Ramesh, A. Ramanand, S. Ponnusamy, C. Muthamizhchelvan, Synthesis and characterization of NiFe₂O₄ nanoparticles and nanorods, *J. Alloys Compd.* 563 (2013) 6–11.
- [23] S. Sobhanardakani, R. Zandipak, R. Sahraei, Removal of Janus Green dye from aqueous solutions using oxidized multi-walled carbon nanotubes, *Toxicol. Environ. Chem.* 95 (2013b) 909–918.
- [24] S. Brunauer, P.H. Emmett, E. Teller, Adsorption of gases in multimolecular layers, *J. Am. Chem. Soc.* 60 (1938) 309–319.
- [25] I. Langmuir, The Adsorption of gases on plane surfaces of glass, mica and platinum, *J. Am. Chem. Soc.* 40 (1918) 1361–1403.
- [26] H. Freundlich, W. Heller, The adsorption of cis-and trans-azobenzene, *J. Am. Chem. Soc.* 61 (1939) 2228–2230.
- [27] M.J. Temkin, V. Pyzhev, Recent modifications to Langmuir isotherms, *Acta. Physio. chim.* 12 (1940) 217–222.
- [28] V.S. Mane, I.D. Deo Mall, V.C. Chandra Srivastava, Kinetic and equilibrium isotherm studies for the adsorptive removal of Brilliant Green dye from aqueous solution by rice husk ash, *J. Environ. Manage.* 84 (2007) 390–400.
- [29] S. Azizian, M. Haerifar, J. Basiri-Parsa, Extended geometric method: A simple approach to derive adsorption rate constants of Langmuir–Freundlich kinetics, *Chemosphere* 68 (2007) 2040–2046.
- [30] G.L. Dotto, M.L.G. Vieira, L.A.A. Pinto, Kinetics and mechanism of tartrazine adsorption onto chitin and chitosan, *Ind. Eng. Chem. Res.* 51 (2012) 6862–6868.
- [31] S. Khodadoust, M. Ghaedi, R. Sahraei, A. Daneshfar, Application of experimental design for removal of sunset yellow by copper sulfide nanoparticles loaded on activated carbon, *J. Ind. Eng. Chem.* 20 (2014) 2663–2670.
- [32] N. Barka, M. Abdennouri, M.E.L. Makhfouk, Removal of Methylene Blue and Eriochrome Black T from aqueous solutions by biosorption on *Scolymus hispanicus* L.: Kinetics, equilibrium and thermodynamics, *J. Taiwan Inst. Chem. Eng.* 42 (2011) 320–326.
- [33] M.D.G. de Luna, E.D. Flores, D.A.D. Genuino, C.M. Futralan, M.W. Wan, Adsorption of Eriochrome Black T (EBT) dye using activated carbon prepared from waste rice hulls—Optimization, isotherm and kinetic studies, *J. Taiwan Inst. Chem. Eng.* 44 (2013) 646–653.
- [34] M. Maghsoudi, M. Ghaedi, A. Zinali, A.M. Ghaedi, M.H. Habibi, Artificial neural network (ANN) method

- for modeling of sunset yellow dye adsorption using zinc oxide nanorods loaded on activated carbon: Kinetic and isotherm study, *Spectrochim. Acta, Part A* 134 (2015) 1–9.
- [35] H. Gao, S. Zhao, X. Cheng, X. Wang, L. Zheng, Removal of anionic azo dyes from aqueous solution using magnetic polymer multi-wall carbon nanotube nanocomposite as adsorbent, *Chem. Eng. J.* 223 (2013) 84–90.
- [36] C. Klett, A. Barry, I. Balti, P. Lelli, F. Schoenstein, N. Jouini, Nickel doped Zinc oxide as a potential sorbent for decolorization of specific dyes, methylorange and tartrazine by adsorption process, *J. Environ. Chem. Eng.* 2 (2014) 914–926.
- [37] K. Dong, F. Qiu, X. Guo, J. Xu, D. Yang, K. He, Adsorption behavior of azo dye Eriochrome Black T from aqueous solution by β -cyclodextrins/polyurethane foam material, *Polym. Plast. Technol. Eng.* 52 (2013) 452–460.
- [38] A. Mittal, L. Kurup, J. Mittal, Freundlich and Langmuir adsorption isotherms and kinetics for the removal of Tartrazine from aqueous solutions using hen feathers, *J. Hazard. Mater.* 146 (2007) 243–248.
- [39] S. Azizian, Kinetic models of sorption: A theoretical analysis, *J. Colloid. Interface Sci.* 276 (2004) 47–52.
- [40] W. Plazinski, W. Rudzinski, A. Plazinska, Theoretical models of sorption kinetics including a surface reaction mechanism: A review, *Adv. Colloid Interface Sci.* 152 (2009) 2–13.
- [41] M. Haerifar, S. Azizian, Fractal-like adsorption kinetics at the solid/solution interface, *J. Phys. Chem. C* 116 (2012) 13111–13119.